Published in "Nature 472: 334–337, 2011"
which should be cited to refer to this work.

Optically-Healable Supramolecular Polymers

Mark Burnworth[1], Liming Tang[1], Justin R. Kumpfer[1], Andrew J. Duncan[2], Frederick L. Beyer[2], Gina L. Fiore[3], Stuart J. Rowan[1] and Christoph Weder[1,3]

[1]Department of Macromolecular Science and Engineering, Case Western Reserve University, 2100 Adelbert Road, Cleveland, Ohio 44106-7202, USA. [2]U.S. Army Research Laboratory, Aberdeen Proving Ground, Maryland 21005-5069, USA. [3]Adolphe Merkle Institute and Fribourg Center for Nanomaterials, University of Fribourg, CH-1700, Fribourg, Switzerland.

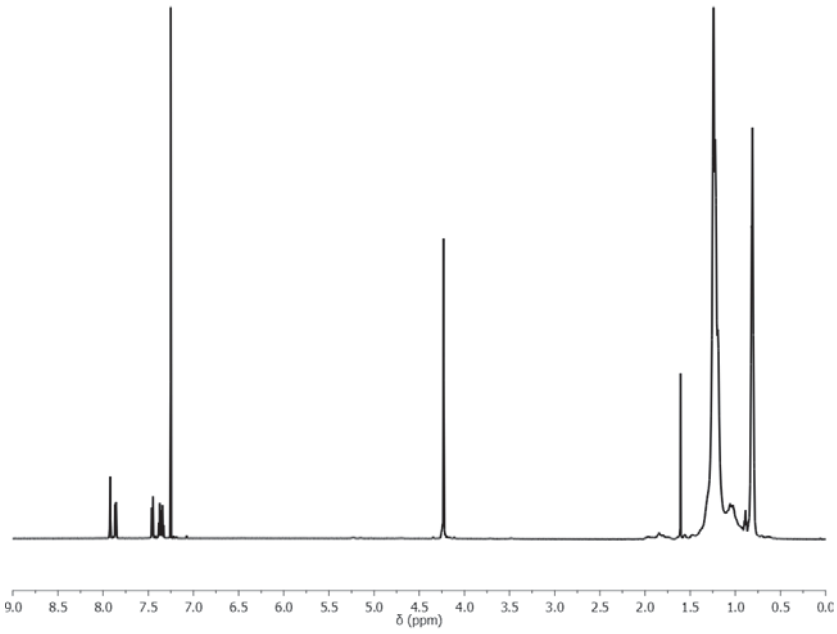

Supplementary Figure S1. Chemical analysis of macromonomer. 600 MHz ^{1}H NMR spectrum of macromonomer **3** in $CDCl_3$.

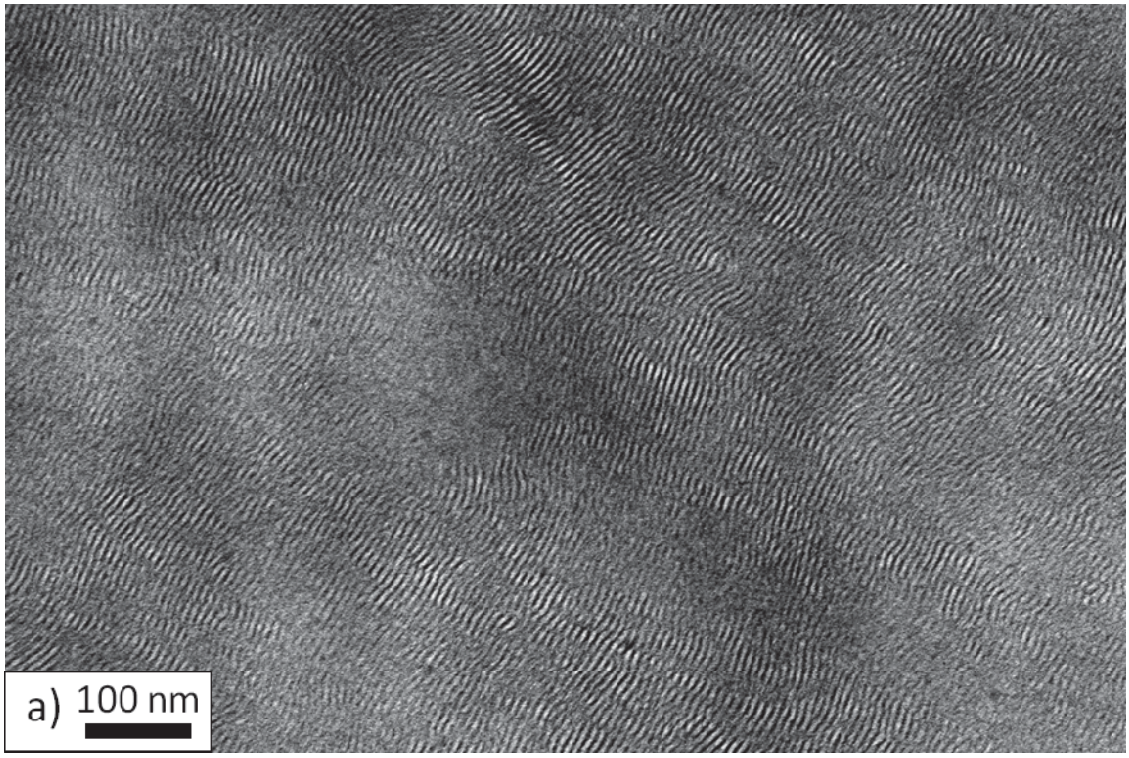

Supplementary Figure S2a. TEM micrograph of 3·[$Zn(NTf_2)_2$]$_{0.9}$.

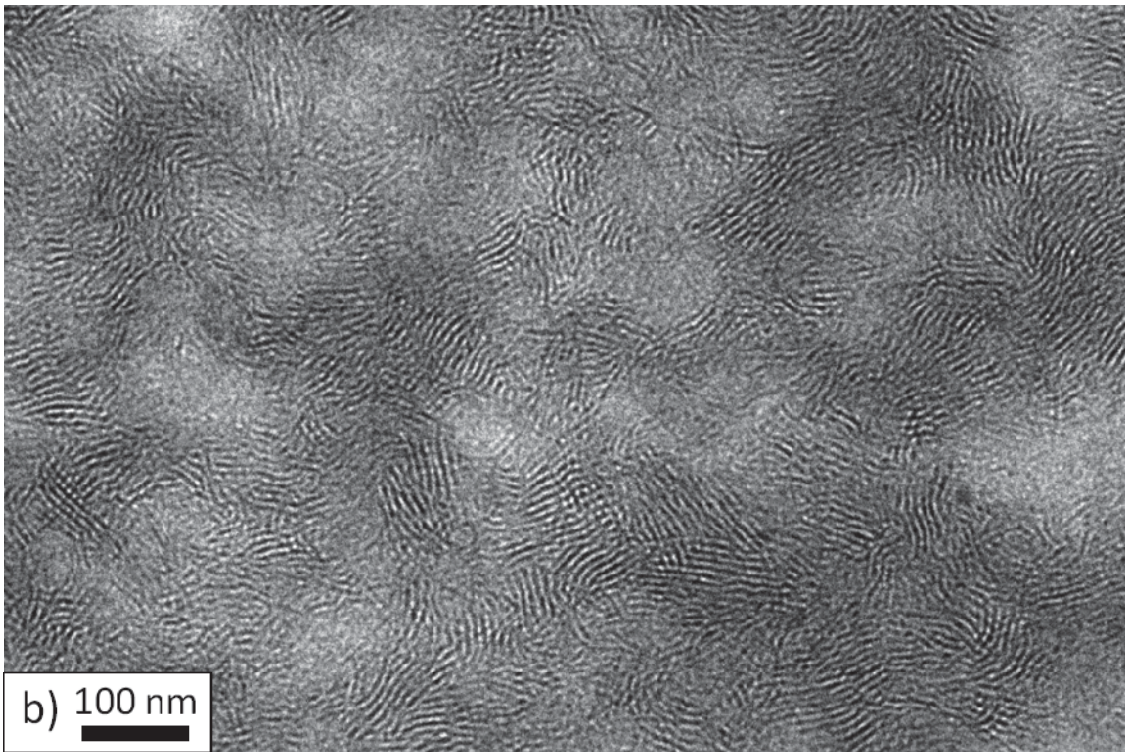

Supplementary Figure S2b. TEM micrograph of 3·[$Zn(NTf_2)_2$]$_{0.8}$.

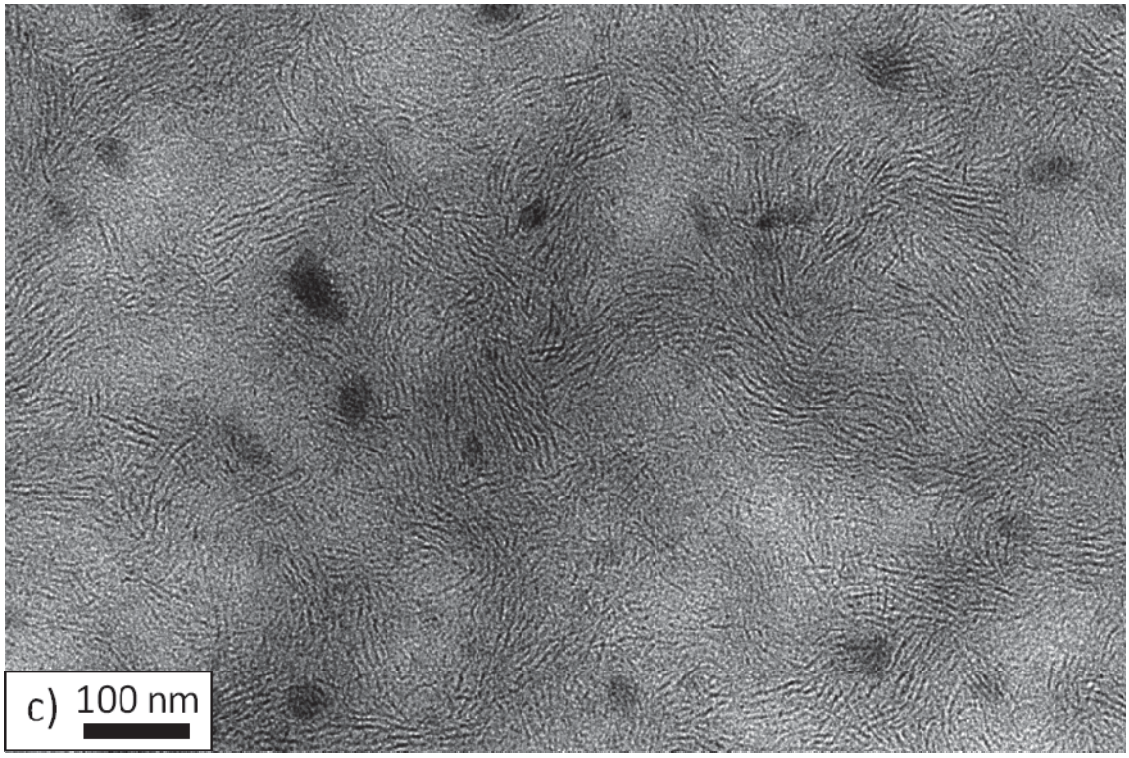

Supplementary Figure S2c. TEM micrograph of 3·$[Zn(NTf_2)_2]_{0.7}$.

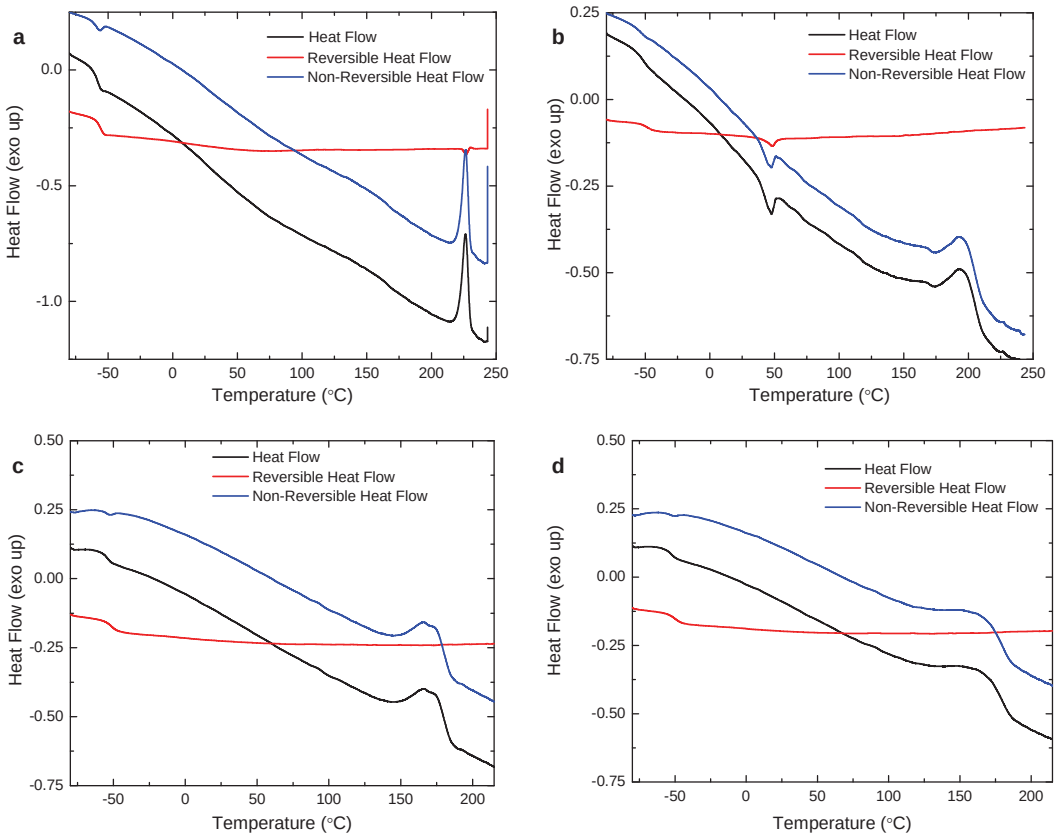

Supplementary Figure S3. Modulated differential scanning calorimetry of starting materials and Zn-based metallo-supramolecular polymers. Modulated DSC traces of **a**, starting material **2**; **b**, macromonomer **3**; **c**, supramolecular metallopolymer **3**·$[Zn(NTf_2)_2]_{1.0}$; and **d**, supramolecular metallopolymer **3**·$[Zn(NTf_2)_2]_{0.7}$. Experiments were conducted at a heating rate of 3 °C/min under nitrogen atmosphere (black, heat flow; red, reversible heat flow; blue, non-reversible heat flow).

Supplementary Discussion. The MDSC trace of **3** shows an irreversible transition at 193 °C, which is also observed in **2** and may be related to reaction of a minor amount of residual double bonds in the poly(ethylene-*co*-butylene) core.

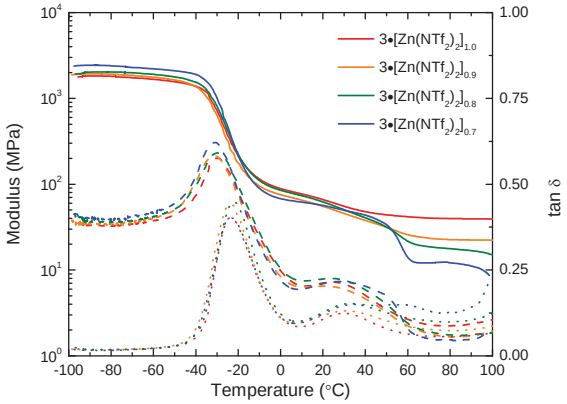

Supplementary Figure S4. Mechanical analysis of Zn-based metallo-supramolecular polymers. Dynamic Mechanical Thermal Analysis (DMTA) traces of films composed of **3** with varying Zn^{2+} ratios (ca. 375 μm in thickness) **3·[Zn(NTf$_2$)$_2$]$_{1.0}$** (red), **3·[Zn(NTf$_2$)$_2$]$_{.0.9}$** (orange), **3·[Zn(NTf$_2$)$_2$]$_{.0.8}$** (green), and **3·[Zn(NTf$_2$)$_2$]$_{.0.7}$** (blue) from -100 to 100 °C; storage modulus (solid), loss modulus (dash), and tan δ (dot). Experiments were conducted under N_2 at a heating rate of 3 °C/min and a frequency of 1 Hz.

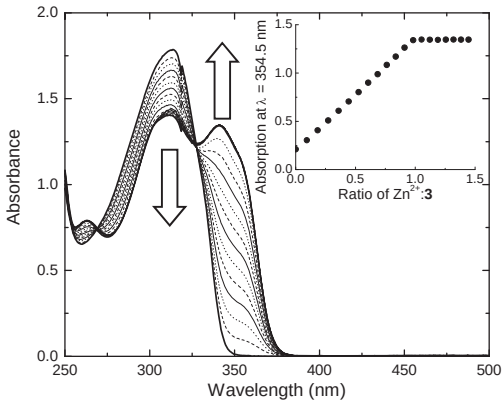

Supplementary Figure S5. Titration of 3 with $Zn(NTf_2)_2$. UV-Vis absorption spectra acquired upon titration of **3** (25 µM) in 9:1 $CHCl_3/CH_3CN$ v/v with $Zn(NTf_2)_2$. Shown are spectra of Zn^{2+}:**3** between ratios of 0 and 1.5. The inset shows the absorption at 354.5 nm as a function of Zn^{2+}:**3**.

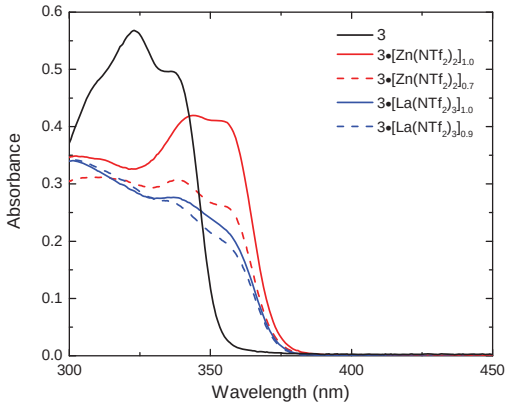

Supplementary Figure S6. Solid-state UV-Vis absorption. UV-Vis absorption spectra acquired for spun-cast thin films from solution (25 mg/mL, 50 µL): **3** (black solid, 2.7 µm), **3·[Zn(NTf$_2$)$_2$]$_{1.0}$** (red solid, 4.9 µm), **3·[Zn(NTf$_2$)$_2$]$_{0.7}$** (red dash, 4.3 µm), **3·[La(NTf$_2$)$_3$]$_{1.0}$** (blue solid, 6.3 µm), and **3·[La(NTf$_2$)$_3$]$_{0.9}$** (blue dash, 4.5 µm).

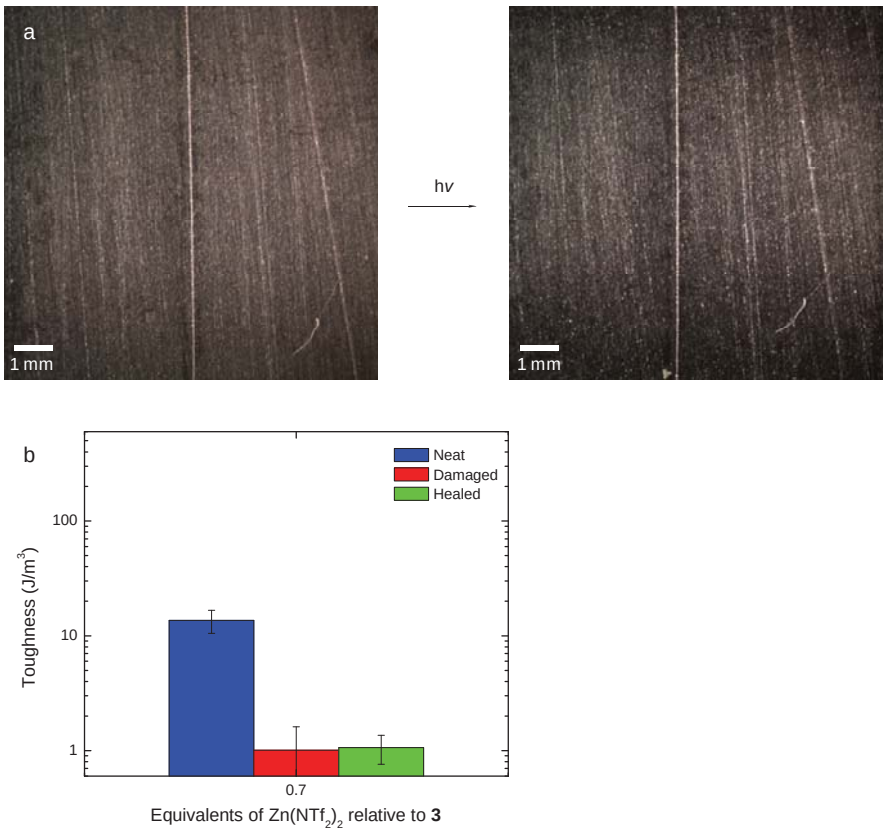

Supplementary Figure S7. Unsuccessful healing attempts with light in the wavelength range from 400-500 nm. a, Optical microscopy pictures of a **3·[Zn(NTf$_2$)$_2$]$_{.0.7}$** film before (left) and after (right) exposure to light in the wavelength range of 400-500 nm of an intensity of ca. 950 mW/cm^2. **b**, Toughness values (*T*) of films of **3·[Zn(NTf$_2$)$_2$]$_{.0.7}$** before and after exposure to light in the wavelength range of 400-500 nm of an intensity of ca. 950 mW/cm^2 (red neat, n=12; green damaged, n=10; blue healed, n=4; errors are s.d.).

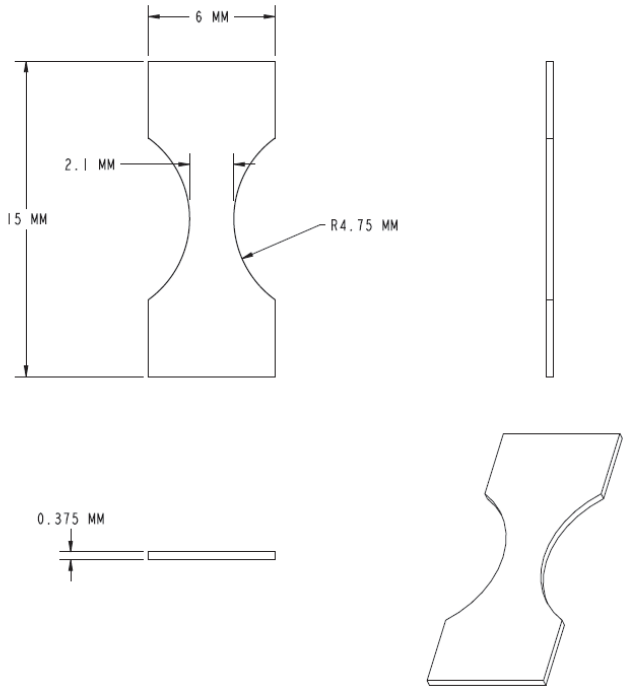

Supplementary Figure S8. Film dimensions for stress-strain experiments. Sample size and dimensions of thin films used in stress-strain experiments. The film thickness ranged from 325-400 μm.

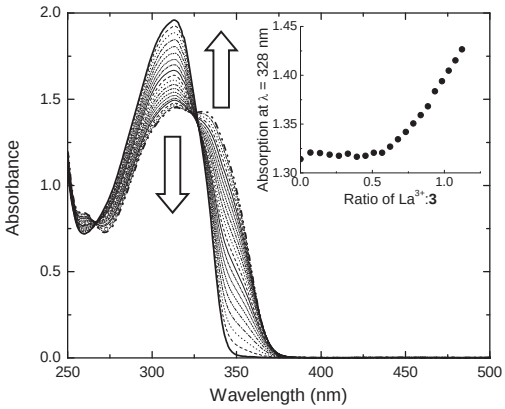

Supplementary Figure S9. Titration of 3 with $La(NTf_2)_3$. UV-Vis absorption spectra acquired upon titration of **3** (25 μM) in 9:1 $CHCl_3/CH_3CN$ v/v with $La(NTf_2)_3$. Shown are spectra of La^{3+}:**3** between ratios of 0 and 1.5. The inset shows the absorption at 354.5 nm as a function of La^{3+}:**3**..

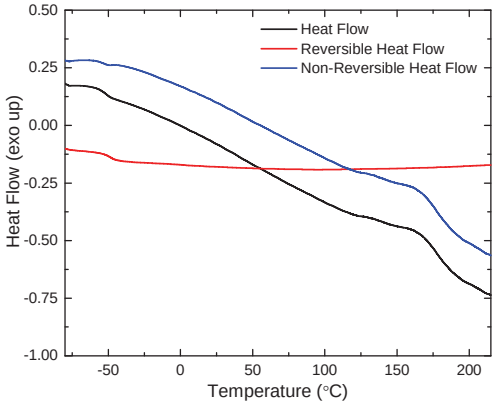

Supplementary Figure S10. Modulated differential scanning calorimetry of metallo-supramolecular polymer 3·[La(NTf$_2$)$_3$]$_{0.9}$. MDSC curves of **3·[La(NTf$_2$)$_3$]$_{0.9}$**. Experiments conducted at a heating rate of 3 °C/min (black, heat flow; red, reversible heat flow; blue, non-reversible heat flow).

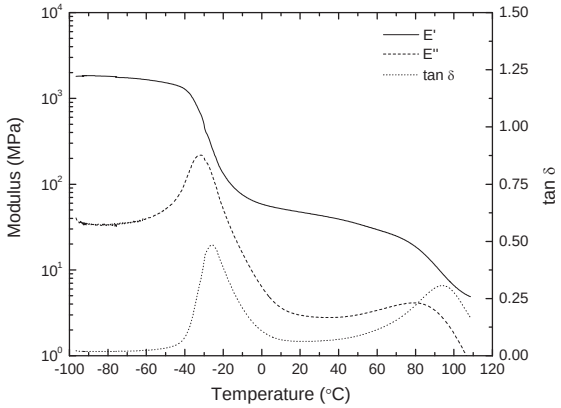

Supplementary Figure S11. Mechanical analysis of La-based metallo-supramolecular polymer. Dynamic Mechanical Thermal Analysis (DMTA) traces of **3·[La(NTf$_2$)$_3$]$_{1.0}$** film (ca. 375 μm in thickness); storage modulus (solid), loss modulus (dash), tan δ (dot). Experiment was conducted under N_2 at a heating rate of 3 °C/min and a frequency of 1 Hz.

Supplementary Discussion. A considerable effort was made to identify dark regions visible in Figure S2c above. These regions were observed in all samples $Zn(NTf_2)_2$ - containing samples, although the regions appeared more frequently in the samples with lower Zn content. The dark appearance of the regions indicates high electron density. The regions were observed before and after staining with RuO_4, indicating that they were not due to some particular concentration of RuO_4. Microanalysis via electron dispersive spectroscopy (EDS) (using an Oxford INCA EDS system with a Si(Li) detector), electron energy loss spectroscopy (EELS, using a Gatan Tridiem GIF system) and energy filtered TEM (EFTEM, using a Gatan Tridiem GIF system) was conducted to determine if the regions were due to a concentration of the supramolecular metallopolymer constituents, but in each case no unusual concentration of the metallo-supramolecular polymers constituents were found. The only characteristic feature of the dark regions observed was a lack of carbon, as illustrated in the EFTEM image below (Supplementary Figure S12b). This lack of organic material, combined with no clear change in the concentration of other compounds associated with the metallo-supramolecular polymers (illustrated by Supplementary Figure 12c), indicates that these dark regions are indicate the presence of an inorganic contaminant unrelated to the metal salts used in the formation of the metallo-supramolecular polymers.

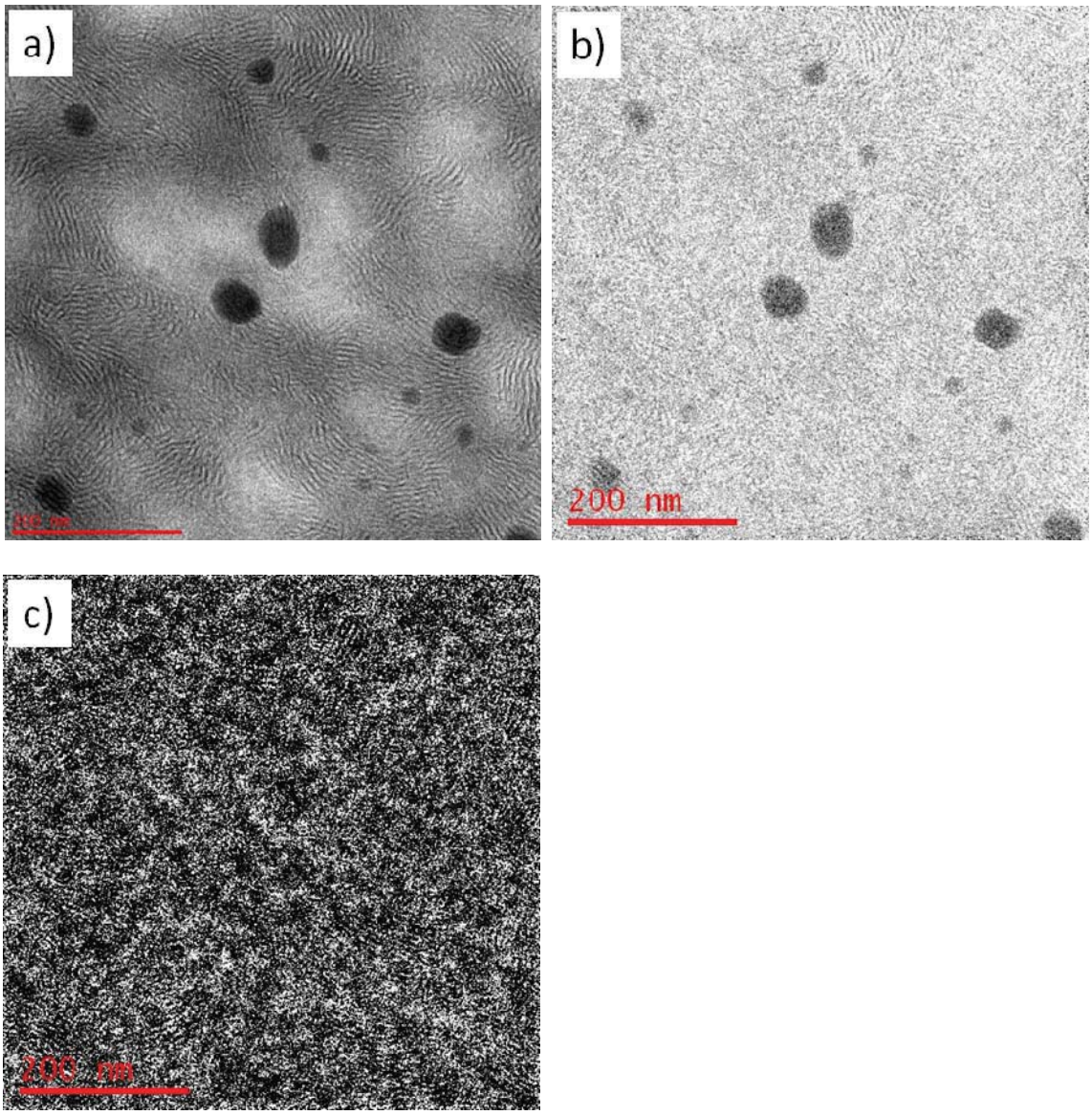

Supplementary Figure S12. TEM dark region analysis. a, A bright field TEM micrograph, **b**, the corresponding EFTEM carbon map in which light regions contain more carbon, **c**, and the corresponding EFTEM sulphur map.

Supplementary Table S1. Results of SAXS data analysis.

Sample	q* (1/Å)	Mean q* (1/Å)	Lamellar period (nm)	Peak width (1/Å)
3·[Zn(NTf$_2$)$_2$]$_{1.0}$	0.0767	0.0755	8.32	0.00437
3·[Zn(NTf$_2$)$_2$]$_{0.9}$	0.0754	0.0734	8.56	0.00425
3·[Zn(NTf$_2$)$_2$]$_{0.8}$	0.0729	0.0703	8.93	0.00674
3·[Zn(NTf$_2$)$_2$]$_{0.7}$	0.0678	0.0676	9.30	0.0122
3·[La(NTf$_2$)$_3$]$_{1.0}$ (melt pressed)	0.0856	0.0845	7.44	0.00412

q* is the scattering angle of the primary Bragg diffraction peak. Mean q* is the average value of q* calculated using the center of the Lorentizian distributions fit to each Bragg diffraction maximum. Lamellar period is calculated as 2π/q using mean q*. Peak width is taken directly from the parameters of the Lorentzian distribution giving the best fit in a least squares analysis.

Supplementary Table S2. Results of stress-strain experiments.

Sample	n	Mean Toughness (J/m^3)	Standard Deviation
3·[Zn(NTf$_2$)$_2$]$_{0.7}$ Neat	12	13.6	3.1
3·[Zn(NTf$_2$)$_2$]$_{0.7}$ Damaged	10	1.0	0.6
3·[Zn(NTf$_2$)$_2$]$_{0.7}$ Healed	11	13.6	3.7
3·[Zn(NTf$_2$)$_2$]$_{0.8}$ Neat	3	35.1	1.5
3·[Zn(NTf$_2$)$_2$]$_{0.8}$ Damaged	5	1.8	1
3·[Zn(NTf$_2$)$_2$]$_{0.8}$ Healed	4	8.8	4.1
3·[Zn(NTf$_2$)$_2$]$_{0.9}$ Neat	3	136.4	17.5
3·[Zn(NTf$_2$)$_2$]$_{0.9}$ Damaged	3	23.8	13.2
3·[Zn(NTf$_2$)$_2$]$_{0.9}$ Healed	3	29.5	11.1
3·[Zn(NTf$_2$)$_2$]$_{1.0}$ Neat	5	337.6	99.7
3·[Zn(NTf$_2$)$_2$]$_{1.0}$ Damaged	4	59.5	7.2
3·[Zn(NTf$_2$)$_2$]$_{1.0}$ Healed	5	59.5	14.5
3·[La(NTf$_2$)$_3$]$_{0.9}$ Neat	13	55.8	8.6
3·[La(NTf$_2$)$_3$]$_{0.9}$ Damaged	10	17.3	9.8
3·[La(NTf$_2$)$_3$]$_{0.9}$ Healed	10	58	6.8
3·[La(NTf$_2$)$_3$]$_{1.0}$ Neat	3	116.8	4.7
3·[La(NTf$_2$)$_3$]$_{1.0}$ Damaged	3	8.6	5.7
3·[La(NTf$_2$)$_3$]$_{1.0}$ Healed	3	85.3	23.9

Toughness values calculated from the integral of the stress-strain curves, based on the undamaged cross-sectional area.

Supplementary Table S3. Results of force-displacement experiments.

Sample	n	Mean Work (J)	Standard Deviation
3·[Zn(NTf$_2$)$_2$]$_{0.7}$ Neat	12	7.90E-03	4.14E-04
3·[Zn(NTf$_2$)$_2$]$_{0.7}$ Damaged	10	5.58E-04	3.33E-04
3·[Zn(NTf$_2$)$_2$]$_{0.7}$ Healed	11	1.02E-03	3.07E-04
3·[Zn(NTf$_2$)$_2$]$_{0.8}$ Neat	3	2.74E-03	1.20E-04
3·[Zn(NTf$_2$)$_2$]$_{0.8}$ Damaged	5	2.05E-04	9.32E-05
3·[Zn(NTf$_2$)$_2$]$_{0.8}$ Healed	4	8.28E-04	4.20E-04
3·[Zn(NTf$_2$)$_2$]$_{0.9}$ Neat	3	1.54E-02	3.10E-03
3·[Zn(NTf$_2$)$_2$]$_{0.9}$ Damaged	3	2.27E-03	1.30E-03
3·[Zn(NTf$_2$)$_2$]$_{0.9}$ Healed	3	2.73E-03	1.07E-03
3·[Zn(NTf$_2$)$_2$]$_{1.0}$ Neat	5	3.15E-02	1.10E-02
3·[Zn(NTf$_2$)$_2$]$_{1.0}$ Damaged	4	4.98E-03	9.31E-04
3·[Zn(NTf$_2$)$_2$]$_{1.0}$ Healed	5	7.42E-03	3.57E-03
3·[La(NTf$_2$)$_3$]$_{0.9}$ Neat	13	4.46E-03	1.71E-03
3·[La(NTf$_2$)$_3$]$_{0.9}$ Damaged	10	9.92E-04	4.24E-04
3·[La(NTf$_2$)$_3$]$_{0.9}$ Healed	10	3.86E-03	1.63E-03
3·[La(NTf$_2$)$_3$]$_{1.0}$ Neat	3	7.90E-03	4.14E-04
3·[La(NTf$_2$)$_3$]$_{1.0}$ Damaged	3	5.58E-04	3.33E-04
3·[La(NTf$_2$)$_3$]$_{1.0}$ Healed	3	6.24E-03	1.10E-03

Work values calculated from the integral of the force-displacement curves, values are not normalized for cross-sectional area.